Journal of the Optical Society of America B
OPTICAL PHYSICS

Specialty optical fiber fabrication: fiber draw tower based on a CO laser furnace

Clarissa M. Harvey,* Korbinian Mühlberger, Taras Oriekhov, Pawel Maniewski, and Michael Fokine

Department of Applied Physics, Royal Institute of Technology, Roslagstullsbacken 21, 114 21 Stockholm, Sweden
**Corresponding author: charvey@kth.se*

Received 16 July 2021; revised 13 October 2021; accepted 25 October 2021; posted 27 October 2021; published 18 November 2021

An experimental, laboratory-scale optical fiber drawing tower based on CO laser heating has been developed and used to fabricate speciality optical fiber. The CO laser was utilized in a symmetric four beam heating system. The localized and responsive heating time of the laser-based furnace was beneficial for manufacturing crystalline core fibers, specifically, silicon core optical fibers. Moreover, the specific absorption properties of the CO laser radiation in silica have been evaluated with the aid of finite element modeling. In comparison to the more traditional CO_2 laser, CO lasers were found to improve temperature uniformity and heating times while minimizing surface evaporation.

https://doi.org/10.1364/JOSAB.437667

1. INTRODUCTION

Optical fibers are fabricated by softening a scaled-up version of the desired fiber, called preform, and drawing the end out into the final thin fiber. Induction furnaces have long been the workhorse of the fiber fabrication industry, supplying vast amounts of energy to heat silica preforms to around 2000°C. This fiber fabrication technique has been heavily optimized to produce enormous quantities of all-silica fiber at high draw speeds up to kilometers per minute. Research focused draw towers tends to work on smaller scales but is usually based on the same induction furnace design. These types of furnaces are an effective means of making silica fiber; however, the large energies and long heating times involved are not necessarily appropriate for alternate materials.

Laser-based heat sources have several advantages over induction furnaces for fiber fabrication. One is that a laser-based furnace has a very localized hot-zone that minimizes the time for thermal interactions between core and cladding materials such as diffusion, dissociation, and oxidization [1]. Another advantage of such a furnace is the compact footprint, while an induction furnace can require large power, cooling, and purging systems. The requirements for cooling or purging of the laser source are typically smaller and have greater flexibility in location, as they can be placed far away from the hot-zone region in the tower. Additionally, the continuous purging and maintenance required for induction furnaces do not apply to laser-based furnaces, as there is no risk of the heating element degrading and contaminating the fiber during a draw.

Laser-based heating has been used in fiber fabrication [2–4] and, perhaps more commonly, in fiber post-processing in the form of tapering [5], twisting [6], or annealing [7] as some examples. These works have all focused on using a CO_2 laser operating at a wavelength of $\lambda = 10.6\ \mu m$ as a heat source. CO_2 lasers are an established technology and are becoming increasingly accessible and affordable. However, as technology progresses, the CO laser is becoming a more viable option. These lasers work at a wavelength of $\lambda = 5.5\ \mu m$ and come with advantages and disadvantages. On one hand, the water absorption at this wavelength attenuates the beam in a normal atmosphere and causes thermal blooming [8]. This requires the lasers to be operated in a dry environment, which is easily achievable in a laboratory environment by enclosing the beam path and purging it with dry air. On the other hand, the benefits of using a CO laser source vindicate the extra considerations required. The absorption properties of the CO laser beam in silica are of particular interest for fiber fabrication. Silica has a much lower absorption coefficient at $\lambda = 5.5\ \mu m$ than at $\lambda = 10.6\ \mu m$, resulting in a greater penetration depth and more even heating of a silica object when irradiated by a CO laser beam.

Here, we present and evaluate a laboratory-sized optical fiber draw tower based on a CO laser as the heating element of the furnace. The laser furnace used a new oscillating four beam heating configuration to uniformly irradiate the target preform. The tower has been used to fabricate multiple optical fibers with various constituent designs. The preforms for the majority of these fibers have been prepared in-house using a complementary preform fabrication system that is also based on CO laser heating [9]. The scope of this paper covers the tower and furnace designs, an evaluation of CO laser heating in this scenario using finite element modeling, and a summary of some of the fibers produced by this tower.

2. DRAW TOWER DESIGN

A. Overview

The overall structure of the fiber draw tower was similar to that of a standard commercial tower and is illustrated in Fig. 1. The main sections included the feeding section, the furnace, the coating system, and the pulling system. The optical fiber draw tower had a small physical footprint of 1.8 m^2 and a height of 2.8 m. All components of the tower communicated with a control program on a computer developed in-house and was written in Python. The full CO laser beam path, the feeder system, and the furnace were sealed in a dry-air environment to reduce the absorption of the 5.5 μm laser beam in ambient humidity. The sealed chamber was pumped with dry air (Kaeser Compressor DC 2.8) and kept at a slightly positive pressure compared to the laboratory environment. This structure had the added benefits of providing a clean and stable environment for fiber drawing as well as shielding against any scattered laser light. After exiting the furnace, the fiber remained in a covered environment until the coating had been applied to reduce contamination of the fiber.

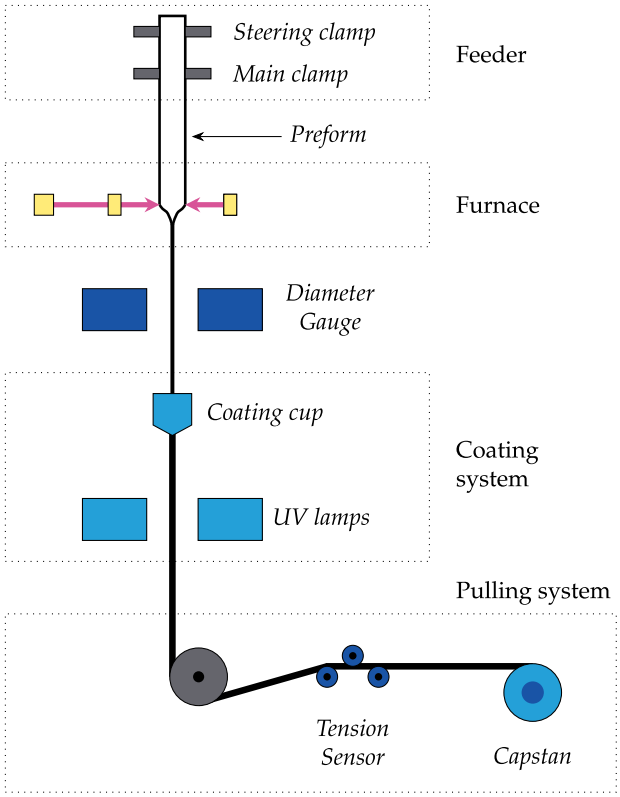

Fig. 1. Side-view schematic of the fiber draw tower. The preform feeder system consisted of an articulated preform clamp and a motorized steering clamp, both of which were mounted on a linear stage that lowered the preform into the furnace. Details of the furnace are given in Section 2.B. The fiber diameter was monitored during fiber draw with the diameter gauge. The coating cup and UV lamps coated and cured a silicone-based coating on the fiber. The fiber was directed with a take-up wheel through a tension sensor and finally onto the capstan. The capstan consisted of a wheel and belt to control the drawing speed (not pictured) and subsequently wind the fiber onto a spool.

The preform feeding system consisted of a vertically mounted motorized (Clearpath-SC) linear stage (Thomson). The preform was mounted on the feeder stage using two clamps. The main clamp held the preform and was articulated. The steering clamp above the main clamp was mounted onto a motorized xy stage. Together with the articulated main clamp acting as a pivot point, this allowed for live steering of the preform, ensuring the preform tip was always centered in the hot-zone. As a consequence, any curvature of the preform could be compensated for during the draw. The feed speed of the preform was set by the control computer and was designed to automatically ramp to the desired feed speed at the beginning of a fiber draw. Furthermore, the feed speed could be controlled to taper the fiber under a constant draw speed. The feeding system pushed the preform into the furnace, softening the glass. The novel furnace design is discussed in detail in Section 2.B. After the furnace, the diameter and ellipticity of the fiber were monitored using a diameter gauge (Zumbach ODAC18XY). The data from the diameter gauge were utilized in an automated feedback loop of the capstan draw speed to control the fiber diameter. The fiber was coated using UV curable silicone (ShinEtsu OF-154 L). The coating was applied at the desired thickness using a coating cup with an adjustable iris bottom. Two UV lamps (OmniCureÂ AC2 series) were positioned on either side of the fiber to ensure even curing of the coating. After the coating was applied the tension of the fiber was measured using a three-wheel tension sensor (Hans-Schmidt FSL-500) placed just prior to the capstan system. These data, read with an interval of 125 ms, were used in a second feedback loop controlling the CO laser power to ensure that the fiber was drawn at the desired tension range. The draw speed was controlled by the capstan (Showmark Pull-N-Spool system). The capstan assembly consisted of a motorized wheel and belt to pull the fiber at a controlled speed. As a final step, the fiber was wound onto the synchronized take-up spool.

B. Furnace Design

The furnace design was based on a CO laser (Coherent Diamond J-3-5) as the heat source. This laser operates at a wavelength of $\lambda = 5.5$ μm. The advantage of using 5.5 μm light is the relatively high penetration depth of this wavelength in silica compared to 10.6 μm radiation of CO_2 lasers currently used for laser heating. The main furnace architecture is shown in Fig. 2. The CO laser beam was incident on a gold mirror mounted on a voice coil (H2W Technologies, Inc. NCM02-17-035-2 F) at 45° relative to the incident beam. The voice coil was driven by a function generator (Keysight 33210 A). The oscillations of the voice coil translated the beam side to side relative to the diffraction grating. The grating split the beam into four separate beams, all in the horizontal plane with a separation angle of 5.17°. The second-order diffracted beams on the outer side contained less power relative to the first-order diffracted beams. This could be compensated for with careful alignment of the beams and the relative position of the preform tip. Four subsequent mirrors (M1 to M4) then directed the beams onto the preform at orthogonal angles. As the voice coil oscillated, the spots incident on the preform swept side to side in unison. At an appropriate driving frequency, the sweep was faster than the thermal response of the preform, ensuring even heating in a

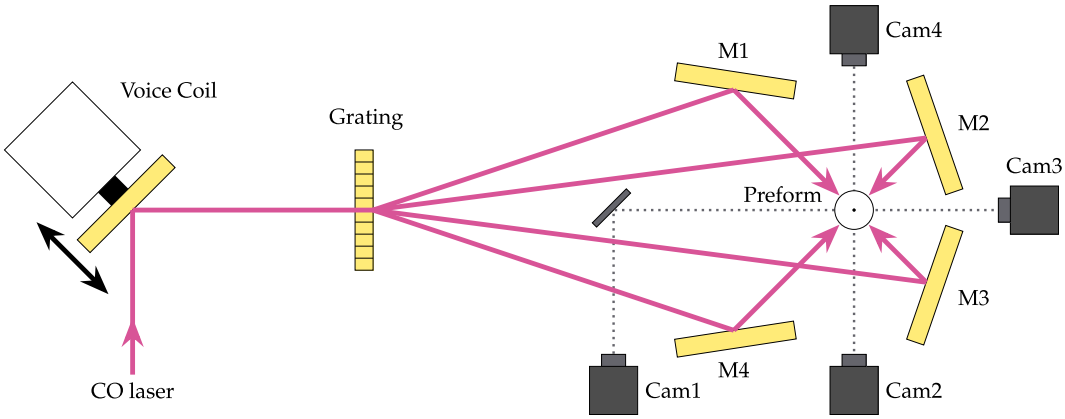

Fig. 2. Top-view schematic of the tower furnace design. The CO laser beam was incident on a gold mirror mounted onto a voice coil. The voice coil was driven by a function generator for the controlled oscillation of the mirror. The CO laser beam was split into four by the grating. All beams were in the horizontal plane. Mirrors (M1–M4) directed the beams onto the preform. The hot-zone was monitored by cameras at orthogonal angles (Cam1–Cam4).

horizontal band around the preform. The $1/e^2$ beam diameter at the preform was approximately 4 mm to 6 mm depending on humidity conditions in the beam path during a draw. To minimize thermal blooming, fiber draws were conducted with a dew point from −35°C to −45°C along the beam path. The laser power was monitored by tapping ≈ 1% of the CO laser beam with a beam splitter. The tapped beam was incident on a thermal power meter (Ophir 7Z02637 Thermal Sensor with NovaII display) measuring with a response time of 800 ms. Depending on preform diameter and draw conditions, the typical total laser power incident on the preform was between 50 W and 150 W during a fiber draw.

The presented furnace design had a relatively open architecture that had the added bonus of visual access to the preform between the gold mirrors. Here, four camera views to monitor all sides of the preform neck-down region during fiber fabrication were installed. An example still from these feeds is shown in Fig. 5. Full inspection of the neck-down region is possible due to monitoring from four orthogonal vantage points. Camera 3 was lowered to provide an additional view of the cooling fiber to monitor fiber centering and any vibration during the draw. Virtual cross-hairs were used on the camera feed during the draw to ensure the fiber remained centered, and any adjustments were made using the motorized steering clamp in the feed system. Camera 4 was raised to monitor the incoming preform (not pictured in Fig. 5) allowing for precise observation of any preform stages or defects as they reached the hot-zone and subsequent fiber. For clarity, the term "hot-zone" is used to describe the volumetric region within the tower where the furnace heat is incident and "hotspot" to refer to the two-dimensional transverse cross section of the preform that lies at the center of the hot-zone.

C. Feedback Loops

1. Fiber Diameter to Draw Speed Stabilization

The diameter of the fiber was controlled during draw using a feedback loop between the diameter gauge and the capstan. The fiber diameter and ellipticity were measured with a resolution of 0.1 μm at an interval of 335 ms. These data were fed into the control computer and used to adjust the draw speed set by the capstan. The response time of the feedback loop could then be adjusted as required for a given fiber draw.

2. Fiber Tension to Laser Power Feedback

An advantage of using a laser-based heat source is the ability to quickly change laser power as needed. A traditional induction furnace requires a long time to heat or actively cool with typical wait times being over several minutes for minor temperature adjustments. Here, the tension was monitored during the draw and fed into a feedback system with laser power. Using the information about the measured tension, the laser power was adjusted to keep the fiber in a specified tension range during the draw. The temperature of the hot-zone was automatically adjusted with an interval of ≈ 1 s optimized for the thermalization time of the preform and change in neck-down shape. This feedback system allows for efficient management of variations in preform shape or composition while keeping the fiber draw conditions constant.

3. HEATING DYNAMICS OF LASER-BASED FURNACES

Silica was the main cladding material considered here as it is an extensively characterized material and a staple of optical fiber fabrication. In the case of the preform diameters of 2 mm to 10 mm used here, both CO and CO_2 laser heating can be considered to be primarily surface heating with conduction transferring the heat through the preform. The silica cladding absorbs the radiation and acts like a crucible heating the core material. A consequence of this heating dynamic is the limit it imposes on the maximum workable preform diameter. A larger thermal mass requires a greater amount of power deposited to achieve the target temperature for drawing. However, as the surface heats, the rate of energy lost to convection, emission, and potential surface vaporization also increases. This results in a finite maximum achievable temperature for a given preform

diameter as the power deposited into the preform reaches equilibrium with the rate of energy lost at the surface. With a large absorption coefficient and preform diameter, the surface could also reach the evaporation temperature of silica at 2973 K before the center is soft enough to draw. In addition, the preform feed rate of the fiber draw is also limited by preform diameter when the heating time exceeds the time in the hot-zone. This can be partially compensated for with an increase of laser power but at the cost of evaporating surface material.

A. Numerical Model of the Preform Thermal Response

Finite element modeling using COMSOL Multiphysics was conducted to investigate the heating dynamics of the preform in this draw tower. These were designed to provide an illustrative example of the heating times and resultant thermal gradients within a preform while being drawn in our furnace design. Another area of interest here was evaluating the differences between CO and CO_2 lasers in this furnace configuration.

For simplicity, a 6-mm-diameter silica rod was considered to evaluate the initial heating conditions in the draw tower and the effects of different absorption mechanics in silica. It is of note that the temperature dynamics will be different for a more complex shape such as the full neck-down structure during a fiber draw, which is beyond the scope needed for this current investigation. In the simulations, four 5-mm-diameter beams were incident on the rod at orthogonal angles. These beams oscillated in unison around the rod using a triangular function with a displacement of 1.5 mm at a frequency of 6 Hz. Convection was modeled as natural convection of a vertical cylinder, and a fit of

$$\varepsilon(T) = -3 \cdot 10^{-7}\,\mathrm{K}^{-2} \cdot T^2 + 2 \cdot 10^{-4}\,\mathrm{K}^{-1} \cdot T + 0.77 \quad (1)$$

was used as the temperature dependant emission of fused silica [10]. The temperature dependent specific heat (in $\mathrm{J\,kg^{-1}\,K^{-1}}$) was

$$c_p(T) = \frac{-2 \cdot 10^5 + T}{23.1992 + T} + 1.7 \cdot 10^{-3}(T + 8 \cdot 10^5), \quad (2)$$

and thermal conductivity of silica (in $\mathrm{W\,K^{-1}\,m^{-1}}$) was

$$\kappa(T) = 0.78 - 0.054 \exp\left(\frac{T+379}{354}\right) + 0.165 \exp\left(\frac{T+379}{405}\right), \quad (3)$$

as obtained from Ref. [11].

The temperature dependent absorption coefficient of the CO_2 laser operating at $\lambda = 10.6$ μm was assumed to be

$$\alpha(T) = \frac{4\pi}{\lambda_{CO_2}}(1.82 \cdot 10^{-2} + 10.1 \cdot 10^{-5}\,\mathrm{K}^{-1}(T - 273.15\,\mathrm{K})), \quad (4)$$

as given in Ref. [12]. As a study of the temperature dependent absorption of a CO laser in silica working at $\lambda = 5.5$ μm was not found, it was estimated using the room temperature value of $\alpha_{RT} = 12787\ \mathrm{m^{-1}}$ [13]. This assumption was verified by running the simulation with an estimated absorption temperature dependence of $10\ \mathrm{m^{-1}\,K^{-1}}$. This changed the thermalization time and increased the equilibrium temperature obtained from the simulation. The effect was found to be small in comparison to the difference in thermalization time between the CO and CO_2 laser furnace simulations and is included in the results presented in Fig. 3. For the purposes of comparing CO to CO_2 lasers in our furnace configuration, a room temperature value of CO laser radiation absorption in silica was deemed adequate. For a more quantitative analysis of laser heating with a CO laser, the full temperature dependent response of the absorption of silica at 5.5 μm is required.

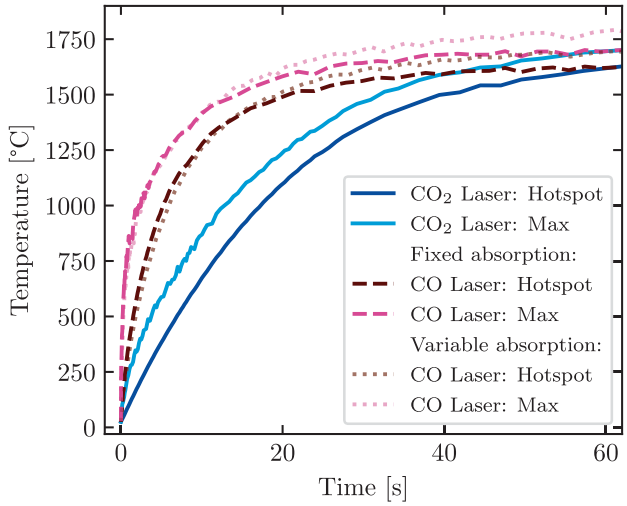

Fig. 3. Comparison of hotspot heating times achievable with CO lasers (dashed lines) and CO_2 lasers (solid lines). Simulations were constructed to have comparable equilibrium hotspot temperatures at the softening point of silica. The hotspot temperatures shown are the average temperature of the preform cross section centered in the laser beam. The maximum temperature is also shown, which corresponds to the surface temperature where the laser is incident. The light dotted lines are the simulation results performed with an estimated temperature dependence of the absorption coefficient of CO laser radiation in silica.

B. Absorption Comparison of CO and CO_2 Laser Radiation in Silica

The main advantage of using a CO laser over the more widely used CO_2 laser is the lower absorption in silica [13]. The lower absorption means that light penetrates further into the material before being absorbed, thus creating a more even heat distribution [14]. A CO_2 laser operating at $\lambda = 10.6$ μm has an absorption depth of 34 μm in silica at room temperature, which decreases to 4 μm at 1800°C [12]. This results in a high energy density at the surface and a large cross-sectional thermal gradient from the surface to the core. The greater the surface temperature, the quicker energy is lost to convection, surface emission, and evaporation. This fundamentally limits the temperature to which the center of the preform could be heated for a given preform size. The CO laser furnace is still susceptible to this fundamental limit. However, due to the greater penetration depth of light, this temperature limit is higher. This allows for higher temperature operation or for processing larger preform diameters compared to using a CO_2 laser.

The difference in heating times between CO and CO_2 laser heating of a preform is a key consideration for the dynamic process of fiber drawing. Figure 3 shows the simulated temporal

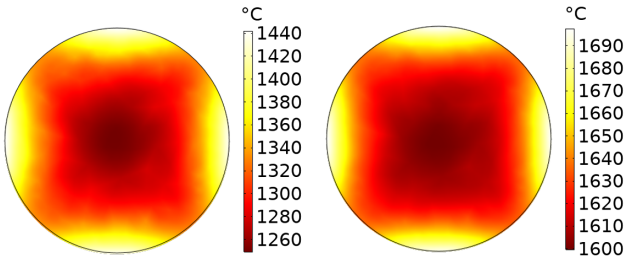

Fig. 4. Simulated transverse temperature gradient in the hotspot of the 6-mm-diameter preform after 11 s (left) and 60 s (right) of CO laser exposure. These times correspond to the temperature response shown in Fig. 3.

response of a 6-mm-diameter silica rod heated by the four beam heating system as described in Section 2.B. The rod starts at room temperature and is exposed to the laser radiation at time $t = 0$ s. The laser power here was treated as a free variable, as losses in the experimental system will vary differently from that of the ideal simulated case for different laser wavelengths. Each simulation was run until the rod reached a thermal equilibrium state at ≈ 1600°C. As the absorption in silica is higher for the CO_2 laser, less power is required to reach the same equilibrium temperature. Thus the simulations with the CO and CO_2 lasers were conducted with a total laser power of $P = 80$ W (20 W per beam) and $P = 4$ W (1 W per beam), respectively. A CO laser power of $P = 80$ W is consistent with the typical laser power used for a fiber draw accounting for mirror losses in the system. The silica rod required more power from the CO laser to reach the same equilibrium temperature, but also reached this temperature much faster than the CO_2 laser case. This implies that by using a CO laser, starting a draw is faster and higher preform feed speeds can be used.

A property of interest is the thermal gradients that exist in the transverse plane of the preform during heating. Each point of the cross section needs to be at a sufficiently high temperature to be soft enough for fiber drawing. If large thermal gradients exist, then parts of the preform may be too viscous for optimum drawing even though the average temperature of the preform in the hot-zone is sufficiently high. Additionally, an even temperature across the transverse plane minimizes distortions in the produced fiber. Figure 4 shows the simulated cross section of the silica rod at different stages during heating. The square symmetry of the temperature distribution rotated with the moving laser beams. Here, two times were chosen where the square symmetry had the same orientation to simplify comparison. After exposing the preform for 60 s to CO laser radiation, the thermal gradients across the preform cross section remained at less than 90°C, which was acceptably small enough for effective fiber drawing.

4. OPTICAL FIBERS PRODUCED

A. Silicon Core Optical Fiber

The specialist nature of this draw tower is designed around the fabrication of innovative optical fibers, namely, hybrid material fibers consisting of a semiconductor or crystalline core with a silica glass cladding. The principle fibers investigated were silicon core optical fibers. These are an important area of research in

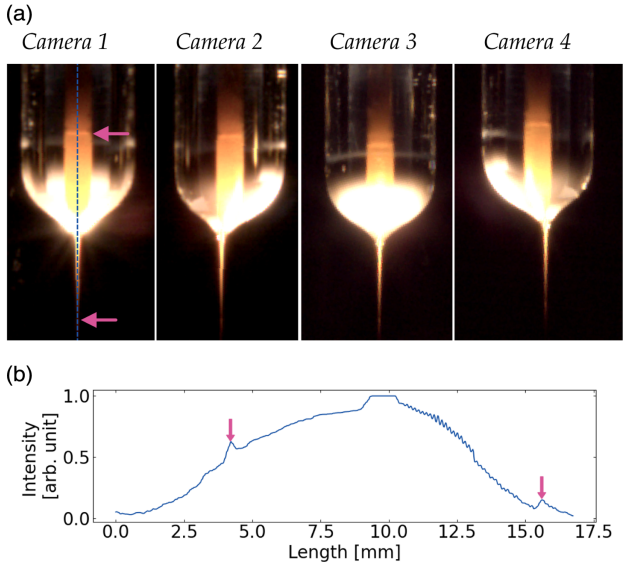

Fig. 5. (a) Example image of the hot-zone region in the draw tower furnace during fiber fabrication. Preform is constituted of a silicon core and silica cladding. Camera placement in the furnace is shown in Fig. 2. (b) Intensity profile measured along the blue dashed line in Camera 1. The peaks in intensity (indicated by pink arrows) show the boundaries of the silicon melt zone.

optics, as the crystalline semiconductor possesses many unique properties not found in all-glass fibers. These fibers support the guidance of longer wavelengths that are beyond the transmission window of silica. The high $\chi^{(3)}$ of silicon and the small mode areas of these optical fibers make them of particular interest in nonlinear optical research. The semiconductor nature also supports electric and optoelectronic properties.

The optical properties of the fiber are dependent on the purity of the silicon and the quality of the silicon crystal. To maintain a high silicon purity, it is important to minimize the heating time of the silicon to reduce the diffusion of oxides or other contaminants into the core while it is in a molten state [1]. A single crystal core is achieved through specific cooling conditions and thermal gradients that prevent the development of multiple nucleation sites within the core [7]. The localized heating of a CO laser furnace is especially suited to meet both of these criteria.

The differing properties of silica and silicon require extra consideration to fabricate an effective optical fiber. The significant material properties here are the thermal expansion and thermal conductivity of the two materials. The anomalous expansion of silicon places substantial stress on the silica cladding as the fiber cools. With excessive stress, the silica cladding may fracture, leading to a dendritic core as the silicon expands into the cracks, or even complete rupture of the fiber, causing a break during fabrication. The higher thermal conductivity of silicon also requires more power to be deposited to heat the same volume of a silicon–silica preform compared to a pure silica preform. The silicon core fibers fabricated here were drawn from a preform manufactured in-house also using a CO laser heating system [9]. The main section of the preform is silicon inside a silica tube. The beginning section of the preform was collapsed into a pure silica rod. This beginning section was used as the drop-off

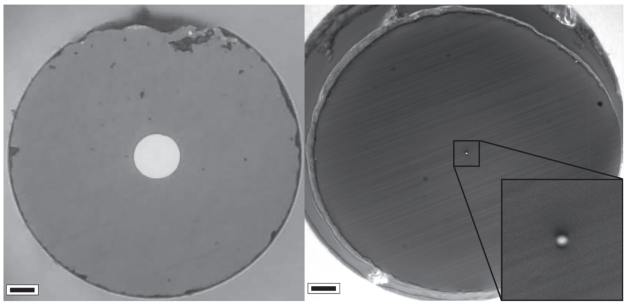

Fig. 6. Polished ends of silicon core optical fibers. (left) 20-µm-diameter core fiber. (right) 1.3-µm-diameter core. Black scale bar is 10 µm.

and stabilization region to ensure the desired drawing parameters were reached before the silicon section of the preform was reached. This reduced wastage and the thermal exposure time of the silicon.

The transition into the silicon-core region leads to a sudden rise in tension due to two reasons: the higher thermal conductivity of silicon compared to silica and the latent heat needed to melt the silicon. Both reduce the temperature of the hotspot. In the worst case, this can lead to a breakage of the fiber. Thus, a fast adjustment in laser power is required to negate this. Section 2.C.2 described the tension feedback loop, which rapidly detects the spike in tension, increases the laser power, and allows for continuing the fiber draw at the desired tension after a short thermalization time of 1 s to 5 s.

The molten silicon is easily visible in the neck-down region when viewed through the furnace cameras. An example image from the live neck-down region feed is shown in Fig. 5. The emissivity of silicon changes with phase, resulting in a darker line being visible at both faces of the molten region. This allowed for real-time monitoring of the stability of the solidification front of the silicon as the cooling fiber exits the hot-zone. The off-center nature of the neck-down visible in cameras 2 and 4 was to compensate for the slight difference in power between the beams of different diffraction orders, which is visible as the two brighter spots on the perform neck-down in camera 3. This configuration minimized the ellipticity of the resultant fiber. Lengths of silicon core fiber of several hundreds of meters in length have been drawn in this draw tower. Additionally, different proportions of silicon have been used to produce several core sizes varying from 1.3 µm to 20 µm in diameter in a 125 µm outer diameter fiber. Micrographs of two of the fibers are shown in Fig. 6. The 20 µm and 1.3 µm core fibers were drawn at speeds of ≈ 1 m min^{-1} and 10 m min^{-1}, respectively, with a tension of ≈ 40 cN.

The silicon fibers drawn here have been characterized to have optical losses of down to 0.2 dB cm^{-1} at 1500 nm (an example cutback measurement is shown in Fig. 7). These values of silicon fiber losses have previously been achieved after post-processing to recrystallize the silicon core [7] and are comparable to established draw tower results [15].

B. Other Optical Fiber Fabrication Tests

Another crystalline core material that has been investigated in this draw tower is sapphire (Al_2O_3). A 125-µm-diameter

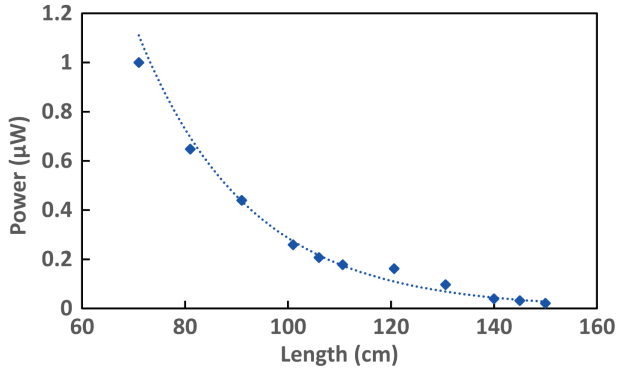

Fig. 7. Example cutback measurement of integrated power over 700 nm to 1800 nm of a 5-µm-diameter silicon core fiber drawn at 10 m min^{-1}. The light source was a Fianium WhiteLase SC480. Blue dashed line is an exponential fit corresponding to a loss of 0.2 dB cm^{-1}.

pure sapphire fiber was inserted into a 6 mm outer and 2 mm inner diameter silica tube and drawn in the tower. Draws were tested both with and without vacuum applied to collapse the hole. Sapphire has a melting point of 2050°C, at which point the silica has a relatively low viscosity. These temperatures were reached in the draw tower, successfully drawing both sapphire derived core and silica cladding simultaneously. Figure 8(a) shows the adhesion between the sapphire derived core (bright crescent shape) and the silica tube. This indicates that the two materials are compatible in this system.

It was found that if the sapphire was heated for too long or the draw temperature was too high, it diffused nearly completely into the silica. Thus there is a narrow temperature window above the sapphire melting point and below the temperature at which diffusion occurs that needs to be met for fiber drawing. The fine control of laser power with a quick response of the tower proved crucial to quickly find draw parameters to prevent full sapphire diffusion while drawing. This draw used a draw

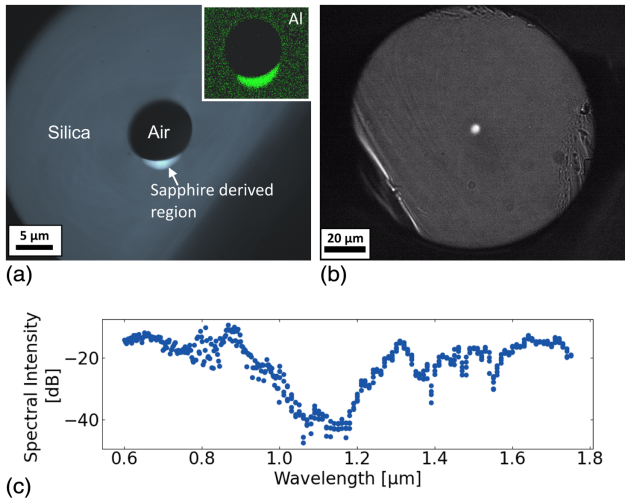

Fig. 8. (a) Bottom lit micrograph of a cleaved end of initial sapphire (Al_2O_3) derived core fiber fabrication test. The draw was a test of material compatibility between sapphire derived region (bright crescent) and the silica capillary. The inset shows the EDS map of aluminium in the central region of the fiber. (b) Micrograph of silica fiber with a Ti-doped core drawn from a preform prepared using glass powder deposition. (c) Transmission spectra of the Ti-doped fiber.

speed of 11.5 m min^{-1} at a tension of 20 cN to 25 cN. Even with material diffusion, a large index step can be achieved in the sapphire derived region of the fiber to form a waveguide [16].

In addition to the target crystalline core fibers, the draw tower has been tested with different types of silica fibers. The draw tower has been used to routinely supply fiber to other in-house research projects. These have included fibers from the more traditional stack and draw style preforms, and multicore fibers from 3D printed preforms such as those fabricated by direct glass powder deposition (DPD). An example fiber drawn from a DPD preform is shown in Fig. 8(b). For the glass DPD preforms, the bulk of material is prepared in-house by DPD using sub-micrometer powders [17]. By careful mixing of dry powders, the mechanical as well as optical properties of the sintered glass were engineered and tailored to application [18] using titania to increase the refractive index of the glass [19]. Here, the silica (fumed silica, Alpha Aesar) and titania powder (TiO_2, anatase, US Research Nanomaterials Inc.) were mixed then sintered using a CO_2 laser beam, and a fully densified glass body was printed. The test preform was assembled using the printed body (12 mm long cylinder with diameter of 1 ± 0.1 mm) inserted into a fused quartz tube (Goodfellow) forming preform's core and cladding, respectively. Subsequently, the preform was drawn into 125 μm fiber at a speed of 7 m/min and a tension of $\approx$ 15 cN. An example transmission is shown in Fig. 8(c). The optical as well as spectroscopic properties of the fibers prepared with DPD are currently under study in our group.

5. DISCUSSION

Overall, the optical fiber draw tower has performed exceedingly well. The scale of the tower and the fundamental constraints of laser heating do limit the quantity of fiber that can be produced in a single draw. While this may not be tolerable for large scale industrial fiber fabrication, it is ideal for fabricating smaller, research scale speciality optical fibers with a large scope of possible fiber designs and materials possible. The small footprint, few maintenance requirements, and relatively quick start-up times have made this a convenient system to have in the laboratory to fabricate and study optical fiber.

Simulations of the furnace tie in with the qualitative behavior observed during fiber draws. From initial laser exposure, a preform drop-off could be achieved within a couple of minutes with modest heating and minimal surface evaporation. For a stable fiber draw, it is beneficial to reach an equilibrium temperature where the power supplied to the silica is balanced with that lost to cooling mechanisms. This has been shown to be more easily achievable using a CO laser than a CO_2 laser. While it is possible to expedite the heating of the preform by applying a higher power initially, this leads to greater surface evaporation and instabilities in drop-off conditions of the draw. The simulations and experimental experience also corroborated the hypothesis that a CO laser was an appropriate heat source for this application.

For the purpose of drawing crystalline optical fibers, different thermal gradients are desired in different directions along the preform and fiber. Minimal thermal gradients are desired in the circular transverse plane to ensure radial uniformity of the resulting fiber. However, large thermal gradients are desired in the axial direction to meet the desired cooling requirements for optimum crystal formation. The simulations confirm that the transverse thermal gradients are sufficiently small even in the large scale of the preform. In the smaller fiber, the transverse thermal gradients are much smaller, as it has a lower thermal mass. The axial thermal gradients are discernible from observing the neck-down region of a silicon fiber draw. Here, the solidification front of the silicon at 1440°C was typically visible at 1 cm to 2 cm from the hot-zone when drawn at 10 m min^{-1}. This equals less than 100 ms after the silicon leaves the hot-zone. The corresponding axial temperature gradient is of the order of hundreds to thousands of kelvin per centimeter. The thermal gradients in the axial direction of the preform are almost symmetrical around the hot-zone. This means that the silicon reaches a molten state only a few millimeters above the center of the hot-zone. These short distances and feed rates of several millimeters per minute minimize interaction time between the molten silicon and the silica cladding.

The optical fibers produced thus far have provided an ample test of the capabilities of the presented fiber draw tower. The larger silicon core sizes demonstrate the versatility of this draw method to produce strong fibers despite the substantial difference in thermal expansion of the materials and the resultant stresses on the interface. Conversely, pushing the limits of small, micrometer-sized, silicon core fibers tested the stability and fine control of the draw process as fluctuations in temperature, fluctuations in draw speed, or large vibrations would cause the small amounts of silicon to break up, forming drips or spheres in the resultant fiber.

Furthermore, the fast thermal response time of the laser furnace does have the advantage of providing precise and automated stabilization of fiber tension. This has proved invaluable for adapting to changes in draw conditions or preform composition during a fiber draw. Traditionally, the target fiber diameter or tapering conditions are controlled by using a constant preform feed speed and adjusting the draw speed. This is not ideal for materials that are sensitive to draw speed and cooling conditions. The fine control of feed speed here in conjunction with the other feedback systems allowed for flexible adjustment of the desired fiber diameter while maintaining a constant draw speed.

There is room for further development of this tower and its CO laser furnace system. Future plans entail refining the tension stabilization systems for higher precision control and refining the furnace configuration for even more uniform temperature distribution in the hot-zone. The main focus is now to push the capabilities of the system with diverse and distinctive fiber designs.

6. CONCLUSION

In conclusion, it has been shown that the presented CO laser-based draw tower is a viable means of fabricating speciality optical fibers. Multiple crystalline core materials have been successfully drawn into fiber. Not only could silicon-core fibers, which are an emerging platform for optoelectronic devices, be drawn, but also sapphire derived core fibers and all-glass optical fibers. This underlines the flexibility of the presented draw tower and its diversity regarding fiber fabrication, making it an

invaluable tool for the development of novel fiber types at an early experimental stage.

Funding. Stiftelsen för Strategisk Forskning (RMA15-0135); Knut och Alice Wallenbergs Stiftelse (2016.0104).

Acknowledgment. We acknowledge Aquiles Carattino who provides vital information for Python programming at www.pythonforthelab.com under the CC BY-NC-SA 4.0 license.

Disclosures. The authors declare no conflicts of interest.

Data Availability. Data underlying the results presented in this paper are not publicly available at this time but may be obtained from the authors upon reasonable request.

REFERENCES

1. U. J. Gibson, L. Wei, and J. Ballato, "Semiconductor core fibres: materials science in a bottle," Nat. Commun. **12**, 3990 (2021).
2. U. C. Paek, "Laser drawing of optical fibers," Appl. Opt. **13**, 1383–1386 (1974).
3. A. Heptonstall, M. A. Barton, A. Bell, G. Cagnoli, C. A. Cantley, D. R. Crooks, A. Cumming, A. Grant, G. D. Hammond, G. M. Harry, J. Hough, R. Jones, D. Kelley, R. Kumar, I. W. Martin, N. A. Robertson, S. Rowan, K. A. Strain, K. Tokmakov, and M. Van Veggel, "Invited article: CO_2 laser production of fused silica fibers for use in interferometric gravitational wave detector mirror suspensions," Rev. Sci. Instrum. **82**, 011301 (2011).
4. M. R. Andreeta and A. C. Hernandes, "Laser-heated pedestal growth of oxide fibers," in *Springer Handbook of Crystal Growth* (Springer, 2010), pp. 393–432.
5. R. Aharoni, L. Bidani, M. Sinvani, and Z. Zalevsky, "Initiatory concept of localized CO_2 laser-based tapering rig for realization of in-fiber devices," Opt. Eng. **51**, 075002 (2012).
6. P. St. J. Russell, R. Beravat, and G. K. L. Wong, "Helically twisted photonic crystal fibres," Philos. Trans. Ser. A **375**, 20150440 (2017).
7. N. Healy, M. Fokine, Y. Franz, T. Hawkins, M. Jones, J. Ballato, A. C. Peacock, and U. J. Gibson, "CO_2 laser-induced directional recrystallization to produce single crystal silicon-core optical fibers with low loss," Adv. Opt. Mater. **4**, 1004–1008 (2016).
8. C. Shi, M. L. Ermold, G. E. Oulundsen, and L. A. Newman, "CO_2 and CO laser comparison of glass and ceramic processing," Proc. SPIE **10911**, 109110M (2019).
9. T. Oriekhov, C. M. Harvey, K. Mühlberger, and M. Fokine, "Specialty optical fiber fabrication: preform manufacturing based on asymmetrical CO laser heating," J. Opt. Soc. Am. B **38**, F130–F137 (2021).
10. J. M. Jones, P. E. Mason, and A. Williams, "A compilation of data on the radiant emissivity of some materials at high temperatures," J. Energy Inst. **92**, 523–534 (2019).
11. A. Grellier, "Characterisation of optical fibre tapering using a CO_2 laser," Ph.d. thesis (University of Kent at Canterbury, 2000).
12. A. D. McLachlan and F. P. Meyer, "Temperature dependence of the extinction coefficient of fused silica for CO_2 laser wavelengths," Appl. Opt. **26**, 1728–1731 (1987).
13. R. Kitamura, L. Pilon, and M. Jonasz, "Optical constants of silica glass from extreme ultraviolet to far infrared at near room temperature," Appl. Opt. **46**, 8118–8133 (2007).
14. S. T. Yang, M. J. Matthews, S. Elhadj, D. Cooke, G. M. Guss, V. G. Draggoo, and P. J. Wegner, "Comparing the use of mid-infrared versus far-infrared lasers for mitigating damage growth on fused silica," Appl. Opt. **49**, 2606–2616 (2010).
15. M. Kudinova, G. Bouwmans, O. Vanvincq, R. Habert, S. Plus, R. Bernard, K. Baudelle, A. Cassez, B. Chazallon, M. Marinova, N. Nuns, and L. Bigot, "Two-step manufacturing of hundreds of meter-long silicon micrometer-size core optical fibers with less than 0.2 dB/cm background losses," APL Photon. **6**, 026101 (2021).
16. P. Dragic, T. Hawkins, P. Foy, S. Morris, and J. Ballato, "Sapphire-derived all-glass optical fibres," Nat. Photonics **6**, 627–633 (2012).
17. P. Maniewski, F. Laurell, and M. Fokine, "Laser cladding of transparent fused silica glass using sub-um powder," Opt. Mater. Express **11**, 3056–3070 (2021).
18. P. Maniewski, C. M. Harvey, T. Oriekhov, F. Laurell, and M. Fokine, "Rapid fabrication of 3D fused silica structures with customized glass composition," in *OPAL* (2021).
19. R. Dylla-Spears, T. D. Yee, K. Sasan, D. T. Nguyen, N. A. Dudukovic, J. M. Ortega, M. A. Johnson, O. D. Herrera, F. J. Ryerson, and L. L. Wong, "3D printed gradient index glass optics," Sci. Adv. **6**, eabc7429 (2020).